PERGAMON

International Journal of Solids and Structures 37 (2000) 4871–4891

INTERNATIONAL JOURNAL OF SOLIDS and STRUCTURES

www.elsevier.com/locate/ijsolstr

Free vibrations of non-circular arches with non-uniform cross-section

Sang Jin Oh[a], Byoung Koo Lee[b,*], In Won Lee[c]

[a]*Department of Civil Engineering, Provincial College of Damyang, Damyang, Chonnam 517-800, South Korea*
[b]*Department of Civil Engineering, Wonkwang University, Iksan, Junbuk 570-749, South Korea*
[c]*Department of Civil Engineering, Korea Advanced Institute of Science and Technology, Taejon 305-701, South Korea*

Received 16 March 1998; in revised form 8 July 1999

Abstract

The differential equations governing free, in-plane vibrations of linearly elastic non-circular arches with non-uniform cross-section are derived and solved numerically to obtain frequencies and mode shapes. Numerical results are presented for the quadratic, parabolic, catenary and elliptic arches with hinged–hinged, hinged–clamped, and clamped–clamped end constraints. Three general taper types for a rectangular section are considered. Experimental measurements of frequencies and their corresponding mode shapes agree closely with those predicted by theory.

Keywords: Free vibration; Non-circular arch; Non-uniform cross-section

1. Introduction

The problem of the free vibration of arches has been the subject of much work due to their many practical applications. The governing equations and the significant historical literature on the in-plane vibrations of elastic arches are reported in the following references and their citations: Den Hartog (1928), Veletsos et al. (1972), Irie et al. (1983), Laura et al. (1988), Gupta and Howson (1994), Kang et al. (1995) and Yildirim (1997). These authors calculated the natural frequencies of circular arches for various boundary conditions. For non-circular arches with uniform cross-section, Volterra and Morell (1960), Romanelli and Laura (1972), Wang and Moore (1973), Wang (1975), Lee and Wilson (1989),

* Corresponding author. Fax: +82-653-857-7204.
E-mail address: bkleest@wonnms.wonkwang.ac.kr (B.K. Lee).

0020-7683/00/$ - see front matter
PII: S0020-7683(99)00194-8

Maurizi et al. (1993) and Wilson and Lee (1995) analyzed the free vibration of arches with various geometries.

For non-circular arches with variable cross-section, Wang (1972) computed only the fundamental extensional frequency of a clamped parabolic arch with variable width and depth by using the Rayleigh–Ritz method; and Gutierrez et al. (1989) calculated only the lowest frequencies in flexure and extension by using polynomial approximations and the Ritz method. Recently, Kawakami et al. (1995) have investigated in-plane and out-of-plane free vibrations of curved members with variable sections. In their paper, the free vibration frequencies have been obtained by using the discrete Green function and the numerical integral method.

The main purpose of this paper is to present both the fundamental and some higher free vibration frequencies for linearly elastic non-circular arches with non-uniform cross-section. The differential equations are derived and solved numerically for the parabolic, catenary and elliptic geometries with hinged–hinged, hinged–clamped, and clamped–clamped end constraints. Although the effects of shear deformation are neglected, the effects of rotatory inertia and in-plane axial deformations are included. Numerical results are presented for quadratic arched members of variable cross-section. Three general taper types for rectangular cross section are selected. The lowest four natural frequencies are presented as functions of three non-dimensional system parameters: the arch rise to span length ratio, the slenderness ratio, and the section ratio. In addition, experiments are described in which the free vibration frequencies and mode shapes of three quadratic parabolic arches were measured; and these results agree quite well with the present numerical studies.

2. Mathematical model

The geometry of the non-circular arch with non-uniform cross-section, symmetric about the crown, is depicted in Fig. 1(a). Its span length, rise, subtended angle, and shape of the middle surface are l, h, α, and $y(x)$, respectively. Its radius of curvature ρ, a function of the co-ordinate x, has an inclination ϕ with the x-axis. The left support is at $\phi = \phi_L$ and the right support is at $\phi = \phi_R$. Shown in Fig. 1(a) are the positive directions of radial and tangential displacements, w and v, and positive direction of the

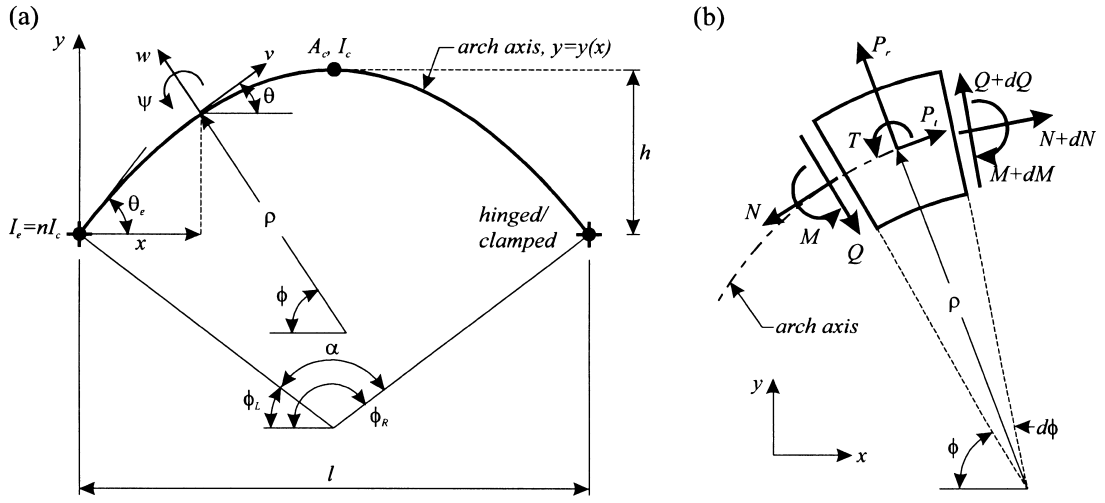

Fig. 1. (a) Arch geometry; (b) loads on an arch element.

rotation angle ψ of the cross-section at point ϕ. The area moments of inertia of cross-section at ϕ, at the crown of arch and at the left/right end are denoted as I, I_c and I_e, respectively. The cross-sectional areas at ϕ and at the crown of arch are depicted as A and A_c, respectively. The angle between the arch axis and the horizontal at the left end support is θ_e, which is equal to half the subtended angle, or $\alpha/2$.

The quantities A and I are expressed in the form

$$A = A_c F, \tag{1a}$$

$$I = I_c G, \tag{1b}$$

where both F and G are functions of the single variable ϕ, as discussed in Section 3.

A small element of the arch shown in Fig. 1(b) defines the positive directions for its loads: the axial forces N; the shear forces Q; the bending moments M; the radial inertia force P_r; the tangential inertia force P_t; and rotatory inertia couple T. With the inertia forces and inertia couple treated as equivalent static quantities, the three equations for "dynamic equilibrium" of the element are

$$\frac{dN}{d\phi} + Q + \rho P_t = 0, \tag{2}$$

$$\frac{dQ}{d\phi} - N + \rho P_r = 0, \tag{3}$$

$$\rho^{-1}\frac{dM}{d\phi} - Q - T = 0. \tag{4}$$

The bending moment and the rotation angle of the cross-section, given by Henrych (1981), are

$$M = -EI\rho^{-2}\left(w'' + w + \rho^{-1}\rho' v\right) = -EI_c G\rho^{-2}\left(w'' + w + \rho^{-1}\rho' v\right), \tag{5}$$

$$\psi = \rho^{-1}(w' - v), \tag{6}$$

where $(') = d/d\phi$, E is the Young's modulus.

The axial force, given by Borg and Gennaro (1959), is

$$N = EA\rho^{-1}(v' + w) - \rho^{-1}M = EA_c F\rho^{-1}(v' + w) - \rho^{-1}M. \tag{7}$$

When Eq. (5) is substituted into Eq. (7), the result is

$$N = EA_c F\rho^{-1}(v' + w) + EI_c G\rho^{-3}\left(w'' + w + \rho^{-1}\rho' v\right). \tag{8}$$

The arch is assumed to be in harmonic motion, or each co-ordinate is proportional to $\sin(\omega t)$, where ω is the angular frequency and t is time. The inertia loadings are then

$$P_r = \gamma A\omega^2 w = \gamma A_c F\omega^2 w, \tag{9}$$

$$P_t = \gamma A\omega^2 v = \gamma A_c F\omega^2 v, \tag{10}$$

$$T = \gamma I\omega^2\psi = \gamma I_c G\omega^2\rho^{-1}(w' - v), \tag{11}$$

where γ is mass density of arch material and $\gamma A = \gamma A_c F$ is mass per unit arc length at any point on the arch.

When Eqs. (5) and (11) are substituted into Eq. (4), then

$$Q = \rho^{-1}\frac{dM}{d\phi} - RT$$

$$= -EI_c\rho^{-3}\left[\left(G\prime - 2G\rho^{-1}\rho\prime\right)\left(w'' + w + \rho^{-1}\rho\prime v\right) + G\left(w''\prime + w\prime + \rho^{-1}\rho'' v - \rho^{-2}\rho\prime^2 v + \rho^{-1}\rho\prime v\prime\right)\right]$$

$$- R\gamma\omega^2 I_c G\rho^{-1}(w\prime - v), \tag{12}$$

where the index $R = 1$ if the rotatory inertia couple T is included, and $R = 0$ if T is excluded.

To facilitate the numerical studies, the following non-dimensional system variables are defined. The arch rise to span length ratio f, the slenderness ratio s and the section ratio n are, respectively,

$$f = \frac{h}{l}, \tag{13a}$$

$$s = \frac{l}{\sqrt{I_c/A_c}}, \tag{13b}$$

$$n = \frac{I_e}{I_c}. \tag{13c}$$

The co-ordinates, the displacements and the radius of curvature are normalized by the span length l:

$$\xi = \frac{x}{l}, \tag{14a}$$

$$\eta = \frac{y}{l}, \tag{14b}$$

$$\delta = \frac{w}{l}, \tag{14c}$$

$$\lambda = \frac{v}{l}, \tag{14d}$$

$$\zeta = \frac{\rho}{l}. \tag{14e}$$

The last is the frequency parameter,

$$C_i = \omega_i s l\sqrt{\frac{\gamma}{E}}, \tag{15}$$

which is written in terms of the ith frequency $\omega = \omega_i$, $i = 1, 2, 3, 4, \ldots$.

When Eqs. (8), (10) and (12) are substituted into Eq. (2) and the non-dimensional forms of Eqs. (13a)–(13c), (14a)–(14e), (15) are used, the result is

$$\lambda'' = s^{-2}a_1\delta'' + \left(a_2 + RC_i^2 s^{-4}a_3\right)\delta' + \left(a_4 + s^{-2}a_1\right)\delta + a_4\lambda' + \left[C_i^2 s^{-2}\left(a_5 + Rs^{-2}a_6\right) + s^{-2}a_7\right]\lambda. \quad (16)$$

When Eqs. (8), (9) and (12) are substituted into Eq. (3) and the non-dimensional forms of Eqs. (13a)–(13c), (14a)–(14e), (15) are used, the result is

$$\delta'''' = a_8\delta''' + \left(a_9 + RC_i^2 s^{-2}a_5\right)\delta'' + \left(RC_i^2 s^{-2}a_{10} + a_8\right)\delta' + \left(a_{11} + s^2 a_{12} + C_i^2 a_{13}\right)\delta + a_{14}\lambda''$$
$$+ \left(a_{15} + RC_i^2 s^{-2}a_{16} + s^2 a_{12}\right)\lambda' + \left(a_{17} + RC_i^2 s^{-2}a_{18}\right)\lambda. \quad (17)$$

The coefficients in the last two equations are

$$a_1 = F^{-1}G\zeta^{-3}\zeta', \quad (18a)$$

$$a_2 = -1, \quad (18b)$$

$$a_3 = F^{-1}G, \quad (18c)$$

$$a_4 = \zeta^{-1}\zeta' - F^{-1}F', \quad (18d)$$

$$a_5 = -\zeta^2, \quad (18e)$$

$$a_6 = -F^{-1}G, \quad (18f)$$

$$a_7 = F^{-1}G\zeta^{-4}\zeta'^2, \quad (18g)$$

$$a_8 = -2G^{-1}G' + 5\zeta^{-1}\zeta', \quad (18h)$$

$$a_9 = -2 - G^{-1}G'' + 5G^{-1}G'\zeta^{-1}\zeta' - 8\zeta^{-2}\zeta'^2 + 2\zeta^{-1}\zeta'', \quad (18i)$$

$$a_{10} = \zeta\zeta' - G^{-1}G'\zeta^2, \quad (18j)$$

$$a_{11} = -1 - G^{-1}G'' + 5G^{-1}G'\zeta^{-1}\zeta' - 8\zeta^{-2}\zeta'^2 + 2\zeta^{-1}\zeta'', \quad (18k)$$

$$a_{12} = -FG^{-1}\zeta^2, \quad (18l)$$

$$a_{13} = FG^{-1}\zeta^4, \quad (18m)$$

$$a_{14} = -\zeta^{-1}\zeta', \quad (18n)$$

$$a_{15} = -2G^{-1}G'\zeta^{-1}\zeta' + 7\zeta^{-2}\zeta'^2 - 2\zeta^{-1}\zeta'', \quad (18o)$$

$$a_{16} = \zeta^2, \tag{18p}$$

$$a_{17} = -G^{-1}G''\zeta^{-1}\zeta' + 7G^{-1}G'\zeta^{-2}\zeta'^2 - 15\zeta^{-3}\zeta'^3 - 2G^{-1}G'\zeta^{-1}\zeta'' + 10\zeta^{-2}\zeta'\zeta'' - \zeta^{-1}\zeta''' - \zeta^{-1}\zeta', \tag{18q}$$

$$a_{18} = G^{-1}G'\zeta^2 - \zeta\zeta'. \tag{18r}$$

The boundary conditions for hinged ends are

$$\lambda = 0, \tag{19a}$$

$$\delta = 0, \tag{19b}$$

$$\delta'' = 0, \tag{19c}$$

where the condition of Eq. (19c) assures that the moment M given by Eq. (5) is zero.

The boundary conditions for clamped ends are

$$\lambda = 0, \tag{20a}$$

$$\delta = 0, \tag{20b}$$

$$\delta' = 0, \tag{20c}$$

where the condition of Eq. (20c) assures that the end rotation ψ given by Eq. (6) is zero.

3. Shape functions: *F* and *G*

The shape functions F and G contained in the governing differential Eqs. (16) and (17) are now defined. Of the two basic classes of arched members, prime and quadratic (Leontovich, 1969), the quadratic arch, considered more economical in bridge construction, is adopted here. Examples are also limited to rectangular cross-sections.

First, the function G is derived for the quadratic arch. A quadratic arch is defined as an arch whose moment of inertia of cross-section varies in accordance with the quadratic equation (Leontovich, 1969):

$$I = \frac{I_c}{\cos\theta\left[1 - \left(1 - \frac{I_c}{I_e\cos\theta_e}\right)\left(\frac{\sin\theta}{\sin\theta_e}\right)^2\right]}. \tag{21}$$

From Fig. 1(a), one obtains

$$\theta = \pi/2 - \phi, \tag{22a}$$

$$\theta_e = \alpha/2. \tag{22b}$$

When Eqs. (22a) and (22b) are substituted into Eq. (21), the result is

$$I = \frac{I_c}{\sin\phi\left(1 + B\cos^2\phi\right)}, \tag{23a}$$

where

$$B = \frac{1}{\sin^2(\alpha/2)}\left[\frac{1}{n\cos(\alpha/2)} - 1\right]. \tag{23b}$$

When Eqs. (1b) and (23a) are combined, the function G can be expressed in terms of the variable ϕ. The result is

$$G = \frac{1}{\sin\phi\left(1 + B\cos^2\phi\right)}. \tag{24a}$$

When Eq. (24a) is differentiated once and twice, the results are

$$G' = G^2\cos\phi\left(2B - 3B\cos^2\phi - 1\right), \tag{24b}$$

$$G'' = 2G'^2G^{-1} + G^2\sin\phi\left(9B\cos^2\phi - 2B + 1\right). \tag{24c}$$

Second, the function F is defined for the three taper types of rectangular cross section. The functions F and F' for rectangular cross-section are expressed in the form

$$F = G^e, \tag{25a}$$

$$F' = eG^{e-1}G'. \tag{25b}$$

In Eqs. (25a) and (25b) the value of e is $e = 1$ for breadth taper, $e = 1/3$ for depth taper, and $e = 1/2$ for square taper (Gupta, 1985).

4. Geometric functions: ϕ, ζ, ζ', ζ'' and ζ'''

The geometric functions ϕ, ζ, ζ', ζ'' and ζ''', contained in the governing differential Eqs. (16) and (17) are computed as follows. The non-dimensional form for the given arch shape $y = y(x)$ is

$$\eta = \eta(\xi). \tag{26}$$

By definition

$$\phi = \frac{\pi}{2} - \tan^{-1}\left(\frac{d\eta}{d\xi}\right), \tag{27}$$

$$\frac{1}{\zeta} = \frac{d^2\eta}{d\xi^2}\left[1 + \left(\frac{d\eta}{d\xi}\right)^2\right]^{-3/2}. \tag{28}$$

Both ϕ and ζ are computed from derivatives of Eq. (26) and are expressed as functions of the single

variable ξ. Then ζ', ζ'' and ζ''' are calculated from the derivatives of Eqs. (27) and (28) by using

$$\zeta' = \left(\frac{\mathrm{d}\zeta}{\mathrm{d}\xi}\right)\left(\frac{\mathrm{d}\xi}{\mathrm{d}\phi}\right), \tag{29a}$$

$$\zeta'' = \left(\frac{\mathrm{d}\zeta'}{\mathrm{d}\xi}\right)\left(\frac{\mathrm{d}\xi}{\mathrm{d}\phi}\right), \tag{29b}$$

$$\zeta''' = \left(\frac{\mathrm{d}\zeta''}{\mathrm{d}\xi}\right)\left(\frac{\mathrm{d}\xi}{\mathrm{d}\phi}\right). \tag{29c}$$

The general equation for the parabolic arch of span length l and rise h is

$$y = -\left(\frac{4h}{l^2}\right)x(x-l), \quad 0 \le x \le l. \tag{30}$$

With Eqs. (13a), (14a) and (14b), the non-dimensional form of Eq. (30) becomes

$$\eta = -4f\xi(\xi - 1), \quad 0 \le \xi \le 1. \tag{31}$$

With Eq. (31), the following geometric functions are calculated from Eqs. (27), (28), (29a)–(29c):

$$\phi = \frac{\pi}{2} - \tan^{-1}\left[-4f(2\xi - 1)\right], \tag{32a}$$

$$\zeta = \left(\frac{1}{8}\right)f^{-1}\left[1 + 16f^{2}(2\xi - 1)^2\right]^{3/2}, \tag{32b}$$

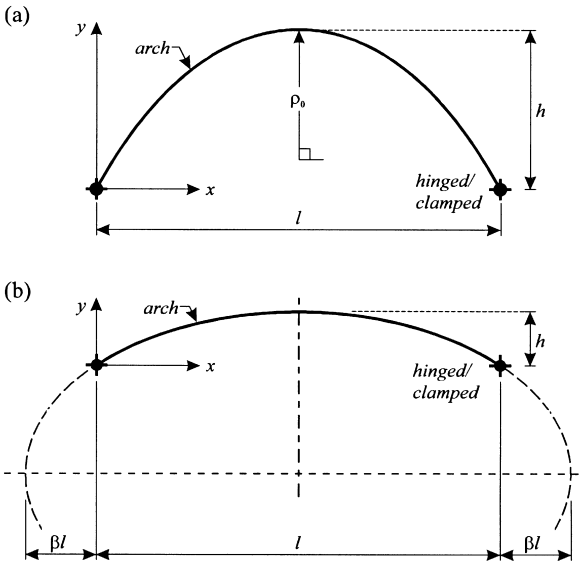

Fig. 2. Arch shapes: (a) catenary; (b) elliptic.

$$\zeta' = \left(\frac{3}{2}\right)(2\xi - 1)\left[1 + 16f^{\,2}(2\xi - 1)^2\right]^{3/2}, \tag{32c}$$

$$\zeta'' = \left(\frac{3}{8}\right)f^{\,-1}\left[1 + 64f^{\,2}(2\xi - 1)^2\right]\left[1 + 16f^{\,2}(2\xi - 1)^2\right]^{3/2}, \tag{32d}$$

$$\zeta''' = 12(2\xi - 1)\left[\frac{11}{8} + 40f^{\,2}(2\xi - 1)^2\right]\left[1 + 16f^{\,2}(2\xi - 1)^2\right]^{3/2}. \tag{32e}$$

Consider the catenary arch shown in Fig. 2(a). This arch has span length l, rise h, radius of curvature at the crown of arch ρ_0, and a co-ordinate system (x, y) originating from the left support. The non-dimensional equation for this arch is

$$\eta = -\zeta_0 \cosh\left(\frac{2\xi - 1}{2\zeta_0}\right) + f + \zeta_0, \quad 0 \le \xi \le 1, \tag{33}$$

where ζ_0 is radius of curvature at the crown of the arch normalized by the span length l.

Substituting $\xi = 1$ and $\eta = 0$ into Eq. (33) leads to

$$\frac{f}{\zeta_0} - \cosh\left(\frac{1}{2\zeta_0}\right) + 1 = 0. \tag{34}$$

For a given f, the corresponding ζ_0 value can be obtained by Eq. (34) by using the bisection method, the method used herein.

Consider now an elliptic arch shown in Fig. 2(b). This arch has span length l, rise h, and a co-ordinate system (x, y) originating from the left support. The corresponding ellipse curve, also shown in Fig. 2(b), is composed of this arch segment and the broken line segments extending from each end. This ellipse curve of semi-major axis $L/2$ and semi-minor axis H is expressed in terms of the (X, Y) co-ordinate system as

Table 1
Comparison of frequency parameter C_i between this study and finite element method (SAP90)

Geometry of arch	i	Frequency parameter, C_i		% Error[a]
		This study ($R = 1$)	SAP90	
Parabolic, hinged–hinged, breadth-taper, $f = 0.1$, $s = 50$, $n = 2$	1	36.21	36.03	0.50
	2	37.16	37.33	0.46
	3	82.61	83.63	1.23
	4	144.6	148.5	2.70
Catenary, hinged–clamped, depth-taper, $f = 0.2$, $s = 100$, $n = 3$	1	43.00	42.71	0.67
	2	88.80	89.38	0.65
	3	129.9	130.1	0.15
	4	162.3	163.8	0.92
Elliptic ($\beta = 0.5$), clamped–clamped, square-taper, $f = 0.3$, $s = 50$, $n = 4$	1	43.63	44.40	1.76
	2	77.16	78.16	1.30
	3	95.06	96.37	1.38
	4	145.6	149.5	2.68

[a] Error = |this study-SAP90|/(this study).

$$\frac{(X+L/2)^2}{(L/2)^2}+\frac{Y^2}{H^2}=1. \tag{35a}$$

The relationships between the two co-ordinate systems of Fig. 2(b) are

$$X=\beta l+x, \tag{35b}$$

$$Y=H-h+y. \tag{35c}$$

Table 2
Effect of rotatory inertia on frequency parameter C_i

Geometry of arch	S	R	Frequency parameter, C_i			
			$i=1$	$i=2$	$i=3$	$i=4$
Parabolic, hinged–hinged, breadth-taper, $f=0.1$, $n=2$	10	0	11.70	32.47	39.76	63.56
		1	11.06 (5.79)[a]	29.99 (8.27)	36.18 (9.90)	60.65 (4.80)
	20	0	17.16	36.27	71.18	83.47
		1	16.90 (1.54)	34.68 (4.58)	70.85 (0.47)	75.84 (10.1)
	30	0	23.58	36.42	83.74	106.2
		1	23.43 (0.64)	35.68 (2.07)	80.01 (4.66)	106.0 (0.19)
	50	0	36.49	37.24	84.03	148.9
		1	36.21 (0.77)	37.16 (0.22)	82.61 (1.72)	144.6 (2.97)
	100	0	36.51	70.15	87.15	149.3
		1	36.44 (0.19)	70.08 (0.10)	86.82 (0.38)	148.2 (0.74)
	200	0	36.52	81.77	148.1	149.3
		1	36.50 (0.05)	81.69 (0.10)	148.1 (0.00)	149.0 (0.20)
Catenary, hinged–clamped, depth-taper, $f=0.2$, $n=3$	10	0	18.23	29.55	47.62	58.85
		1	17.10 (6.61)	29.04 (1.76)	39.99(19.1)	57.64 (2.10)
	20	0	27.37	42.34	67.01	94.08
		1	26.88 (1.82)	40.83 (3.70)	65.74 (1.93)	85.53 (10.0)
	30	0	36.94	44.73	94.45	98.84
		1	36.51 (1.18)	44.02 (1.61)	90.51 (4.35)	97.66 (1.21)
	50	0	42.52	61.50	97.52	154.3
		1	42.19 (0.78)	61.31 (0.31)	95.77 (1.83)	151.9 (1.58)
	100	0	43.09	89.13	130.1	163.6
		1	43.00 (0.21)	88.80 (0.37)	129.9 (0.15)	162.3 (0.80)
	200	0	43.18	91.81	163.0	233.8
		1	43.16 (0.05)	91.71 (0.11)	162.7 (0.18)	233.4 (0.17)
Elliptic ($\beta=0.5$), clamped–clamped, square-taper, $f=0.3$, $n=4$	10	0	23.49	27.82	50.26	54.69
		1	22.36 (5.05)	27.25 (2.09)	43.18 (16.4)	53.29 (2.63)
	20	0	36.03	41.13	68.29	89.64
		1	35.56 (1.32)	40.06 (2.67)	66.72 (2.35)	83.36 (7.53)
	30	0	43.16	50.19	92.34	97.47
		1	42.51 (1.53)	49.87 (0.64)	88.79 (4.00)	96.71 (0.79)
	50	0	43.90	77.54	96.25	148.5
		1	43.63 (0.62)	77.16 (0.49)	95.06 (1.25)	145.6 (1.99)
	100	0	44.16	90.13	153.1	161.8
		1	44.09 (0.16)	89.80 (0.37)	152.0 (0.72)	161.7 (0.06)
	200	0	44.22	90.74	153.3	226.7
		1	44.21 (0.02)	90.65 (0.10)	153.0 (0.20)	226.1 (0.27)

[a] Values in parentheses represent % difference.

When Eqs. (35b) and (35c) are combined with Eqs. (35a), (13a), (14a) and (14b), the general equation for the elliptic arch in non-dimensional form can be expressed in terms of the parameters f and β where $(2\beta+1)l$ is the length of the major axis of the ellipse as shown in Fig. 2(b). The result is

$$\eta = \frac{c_2}{c_1}\left[c_1^2 - \left(\frac{2\xi-1}{2}\right)^2\right]^{1/2} + f - c_2, \quad 0 \le \xi \le 1, \tag{36a}$$

where

$$c_1 = \frac{1+2\beta}{2}, \tag{36b}$$

$$c_2 = \frac{f}{1 - \dfrac{2\left(\beta+\beta^2\right)^{1/2}}{1+2\beta}}. \tag{36c}$$

In the last two curves, ϕ, ζ, ζ', ζ'' and ζ''' are calculated in a straightforward manner from Eqs. (33) and (36a)–(36c), respectively, with use of Eqs. (27), (28), (29a)–(29c).

5. Numerical methods and computed results

Based on the above analysis, a general FORTRAN computer program was written to calculate the frequency parameters $C_i (i = 1, 2, 3, 4)$ and the corresponding mode shapes $\delta = \delta_i(\xi)$ and $\lambda = \lambda_i(\xi)$. The numerical methods described by Veletsos et al. (1972), and Lee and Wilson (1989) were used to solve the differential Eqs. (16) and (17), subject to the end constraints selected from Eqs. (19a)–(19c) and (20a)–(20c). The hinged–hinged, hinged–clamped and clamped–clamped end constraints were considered for

Table 3
Comparison of computed and measured results (parabolic, breadth-taper, $f = 0.25$, $s = 200$, $n = 1.5$, $R = 1$)

		Theory		Experiment	
End constraint	i	C_i	f_i (Hz)	f_i (Hz)	% Deviation[a]
Hinged–hinged	1	26.71	311.4	297	−4.6
	2	64.99	757.8	684	−9.7
	3	117.6	1371.0	1100	−19.8
	4	183.7	2142.0	2049	−4.3
Hinged–clamped	1	33.71	393.1	364	−7.4
	2	75.83	884.2	777	−12.1
	3	132.5	1545.0	1215	−21.4
	4	201.5	2350.0	2121	−9.7
Clamped–clamped	1	42.41	494.5	460	−7.0
	2	87.51	1020.0	916	−10.2
	3	148.6	1733.0	1555	−10.3
	4	219.3	2557.0	2290	−10.4

[a] Deviation = (Experiment − Theory)/Theory.

each of the three arch geometries, for the three general taper types, for given parameters f, s, n, R ($=0$ or 1) and β. (Recall that β is needed for elliptic geometry only.)

First, the Determinant Search method was used to calculate the frequency parameters C_i, and then the Runge–Kutta method was used to calculate the mode shapes. In this study, the four lowest values of C_i and the corresponding mode shapes were calculated. The numerical results, given in Tables 1–3 and Figs. 3–9, are summarized as follows.

In Table 1, values of C_i are presented for parabolic, catenary and elliptic arches. Comparisons are made between C_i computed using the present analysis with $R = 1$ and C_i computed with the packaged finite element program SAP90. For the latter calculations, 100 three-dimensional finite beam elements

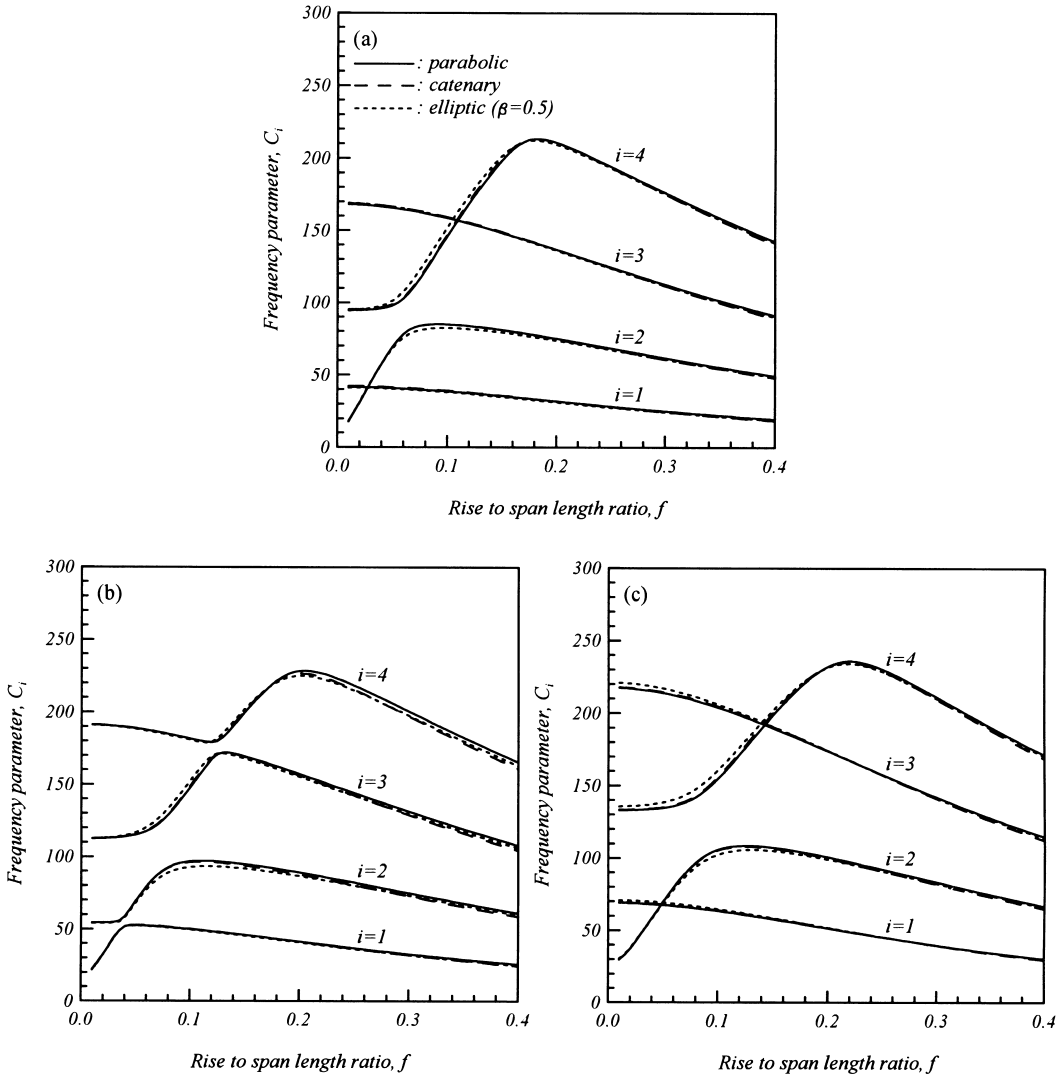

Fig. 3. Effect of f on frequency: (a) hinged–hinged; (b) hinged–clamped; (c) clamped–clamped. Depth-taper;$s = 200$; $n = 2$.

were used and effects of shear area were not included. Comparing the results for like arch parameters, the results for C_i agree to within 2%. The remainder of the numerical results are based on the present analysis.

Table 2 shows the effect of rotatory inertia on the four lowest frequency parameters of three arch geometries. The inclusion of rotatory inertia is to always depress the natural frequencies. This effect becomes more significant as the slenderness ratio decreases.

The results shown in Figs. 3–5, for parabolic, catenary and elliptic arches with $R = 1$, depict the variation of C_i $(i = 1, 2, 3, 4)$ with f, s and n, respectively. The results of these studies may be summarized as follows: (1) The arch geometry has little effect on the frequency parameters. (2) In Figs.

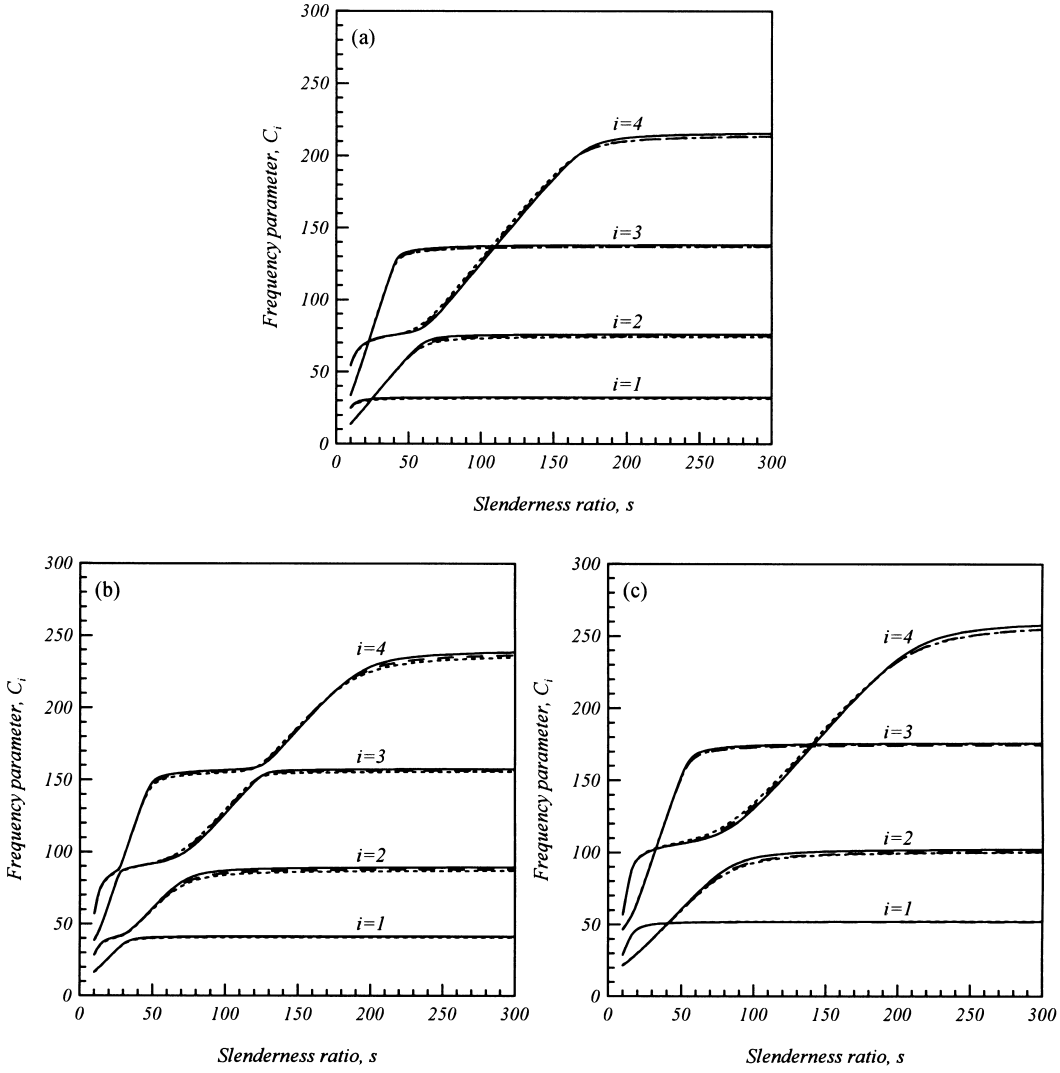

Fig. 4. Effect of s on frequency: (a) hinged–hinged; (b) hinged–clamped; (c) clamped–clamped. Key as Fig. 3; $f = 0.2$; $n = 2$.

3(a), (c) and 4(a), (c), the cross-over points represent two coincident natural frequencies, one corresponding to the symmetric mode and the other to the antisymmetric mode. (3) As the end constraint increases on all three arch geometries, from hinged–hinged to hinged–clamped to clamped–clamped, each value of C_i increases, other parameters remaining constant. (4) Fig. 3 exhibits the common feature that as each arch becomes flat (f approaches zero) the frequency parameters approach those of the straight beam with matched end conditions. (5) As the slenderness ratio s increases to 300, the C_i values approach horizontal asymptotes. When the frequency curves are horizontal, the vibration modes may be almost purely flexural as in a straight beam. (6) As the section ratio n increases (by increasing I_e), the C_i values always increase.

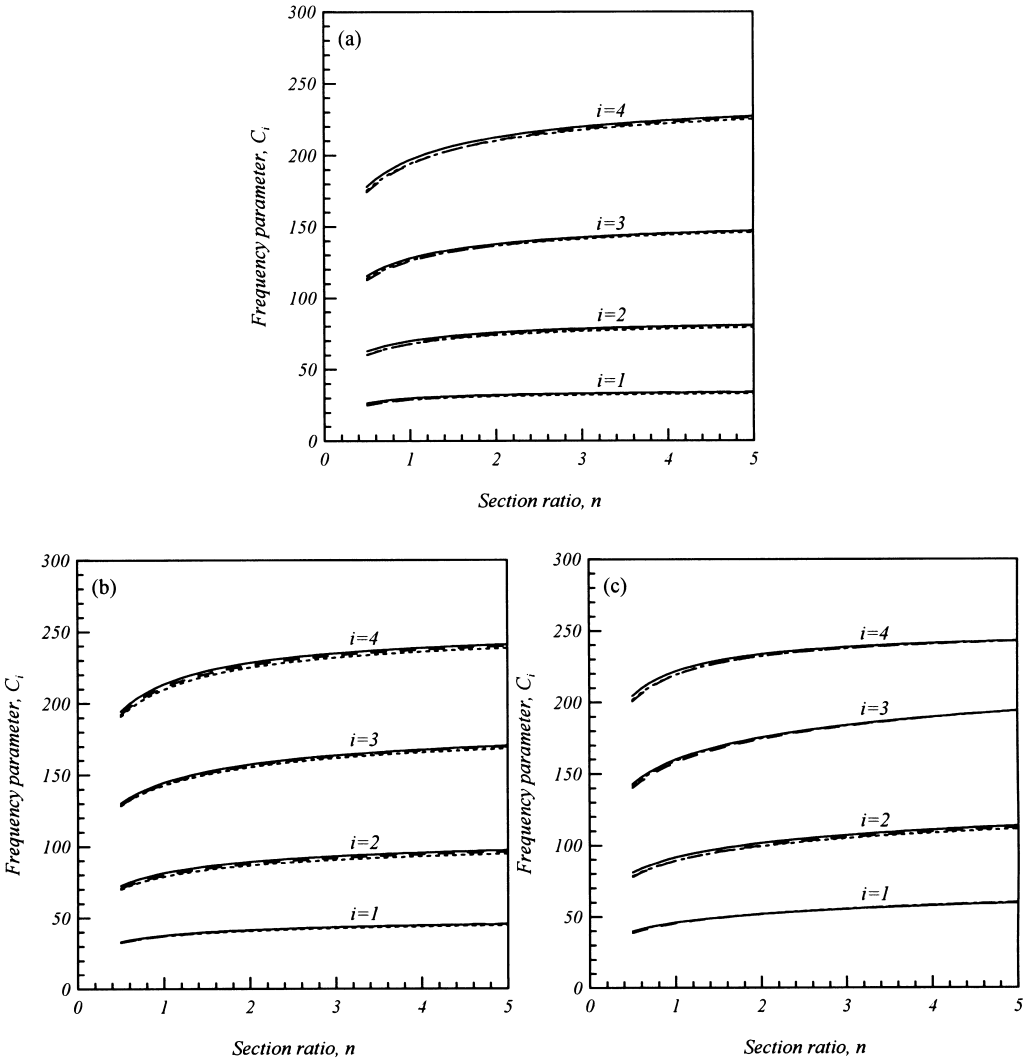

Fig. 5. Effect of n on frequency: (a) hinged–hinged; (b) hinged–clamped; (c) clamped–clamped. Key as Fig. 3; $f = 0.2$; $s = 200$.

The results shown in Figs. 6–8, for breadth, depth and square tapered parabolic arches with $R = 1$, depict the variation of C_i ($i = 1, 2, 3, 4$) with f, with s, and with n, respectively. In these Figures, the C_i values generally increase as the type of taper changes from the breadth to the square to the depth taper.

Shown in Fig. 9 are the computed frequency parameter C_i ($i = 1, 2, 3, 4$) and their corresponding mode shapes for the parabolic arches with hinged–hinged, hinged–clamped and clamped–clamped end constraints for which $e = 1$ (breadth taper), $f = 0.25$, $s = 200$, $n = 1.5$ and $R = 1$. These arch parameters are those chosen for the experimental arches discussed in the next section. The mode shapes for the hinged–hinged and clamped–clamped cases showed the alternating pattern between antisymmetric and symmetric mode shapes as i increased from 1 to 4. However, the mode shapes for the hinged–clamped case were asymmetric mode shapes, which is to be expected since the end constraints are different.

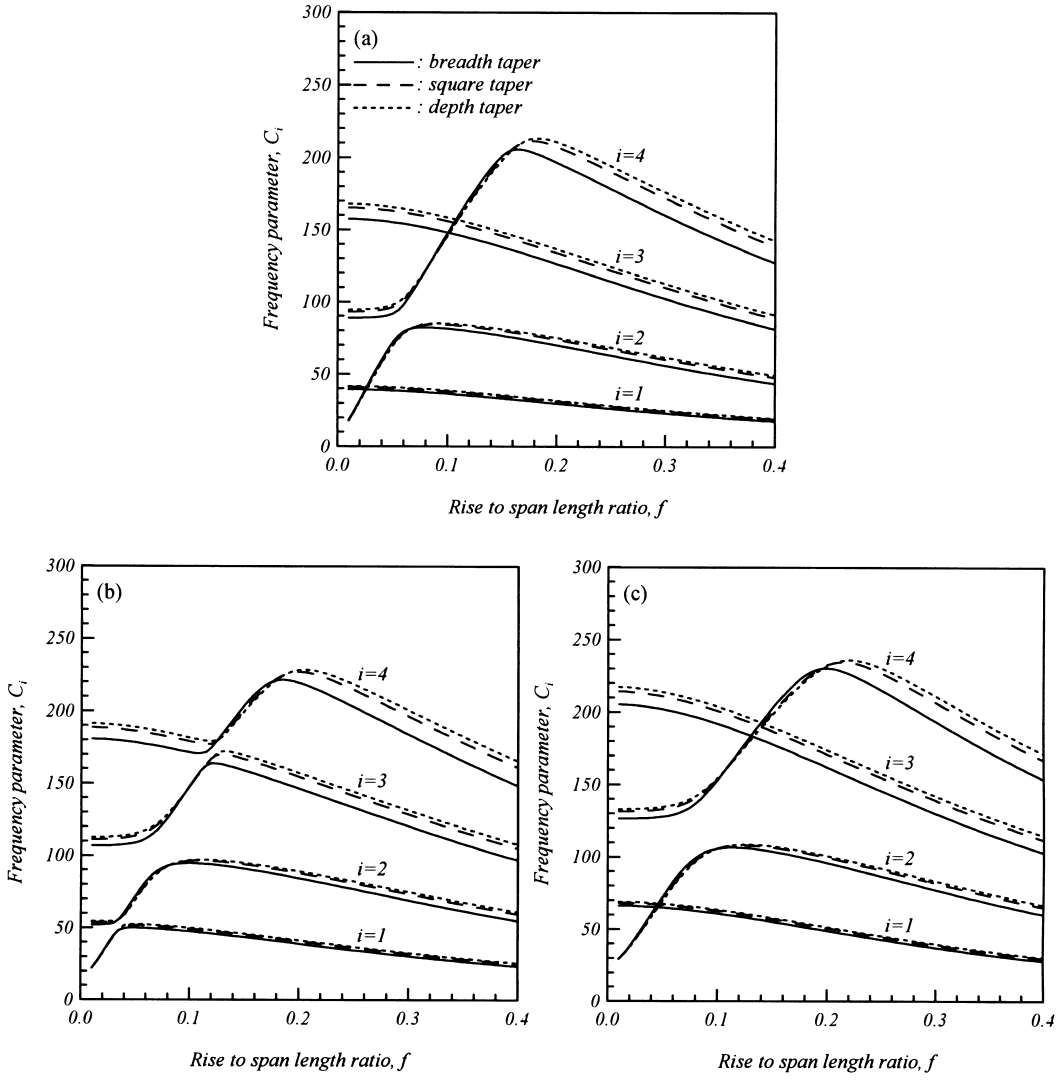

Fig. 6. Effect of f on frequency for parabolic arches: (a) hinged–hinged; (b) hinged–clamped; (c) clamped–clamped. $s = 200$; $n = 2$.

6. Experimental results

Experiments were designed to measure the lowest few free vibration frequencies and mode shapes on three aluminum, laboratory-scale parabolic, tapered arches: a hinged–hinged, a hinged–clamped and a clamped–clamped configuration. These arches had the same geometry: quadratic arches described by Eq. (21), with breadth taper. The dimensions, defined in Fig. 1, were: $l = 34.64$ cm, $h = 8.66$ cm. The depth of the rectangular cross-section of 0.6 cm is constant, and the width of cross-section at the crown of the arch and at the left/right ends are 2.0 and 3.0 cm, respectively. The corresponding non-dimensional parameters were thus $f = 0.25$, $s = 200$ and $n = 1.5$. Based on the methods described above, in which

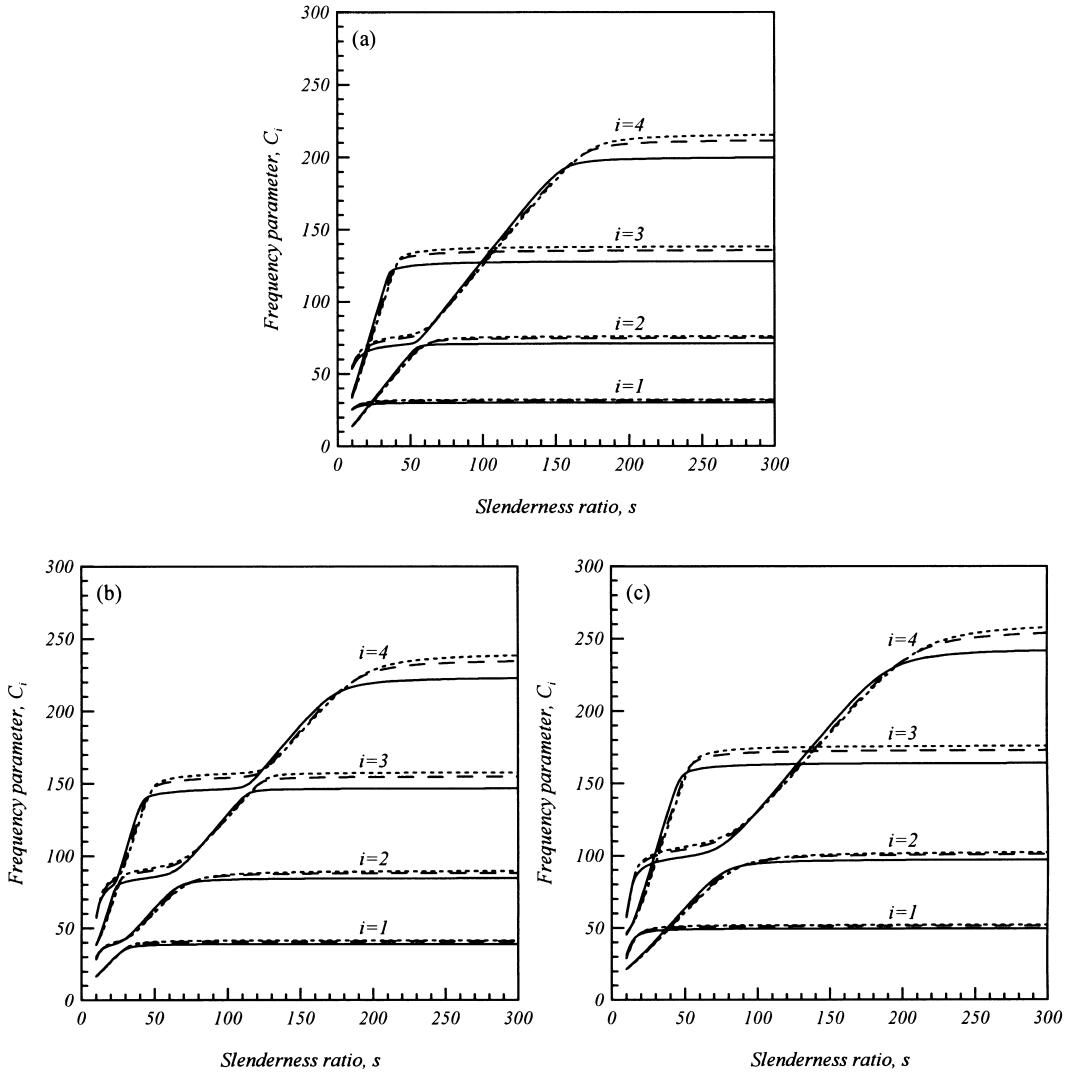

Fig. 7. Effect of s on frequency for parabolic arches: (a) hinged–hinged; (b) hinged–clamped; (c) clamped–clamped. Key as Fig. 6; $f = 0.2$; $n = 2$.

rotatory inertia was included ($R = 1$), the frequency parameters C_i were calculated. The corresponding frequencies ω_i (rad/s) were computed from Eq. (15) based on the following material properties for the aluminum arches: a Young's modulus E of 6.89×10^{10} N/m^2 and a mass density γ of 2680 kg/m^3. The resulting frequencies $f_i = \omega_i/(2\pi)$ Hz, $i = 1, 2, 3, 4$ are given in Table 3 for each of the three arches tested.

The experimental setup and methods of measuring the free vibration frequencies of these three arches is fully described by Lee and Wilson (1989). For the sake of completeness, these methods are now summarized. At each end, the arch was either hinged or clamped to an 80 kgf, isolated granite block where each block "floated" on a rubber pad. Including the end points, 15 reference points evenly spaced

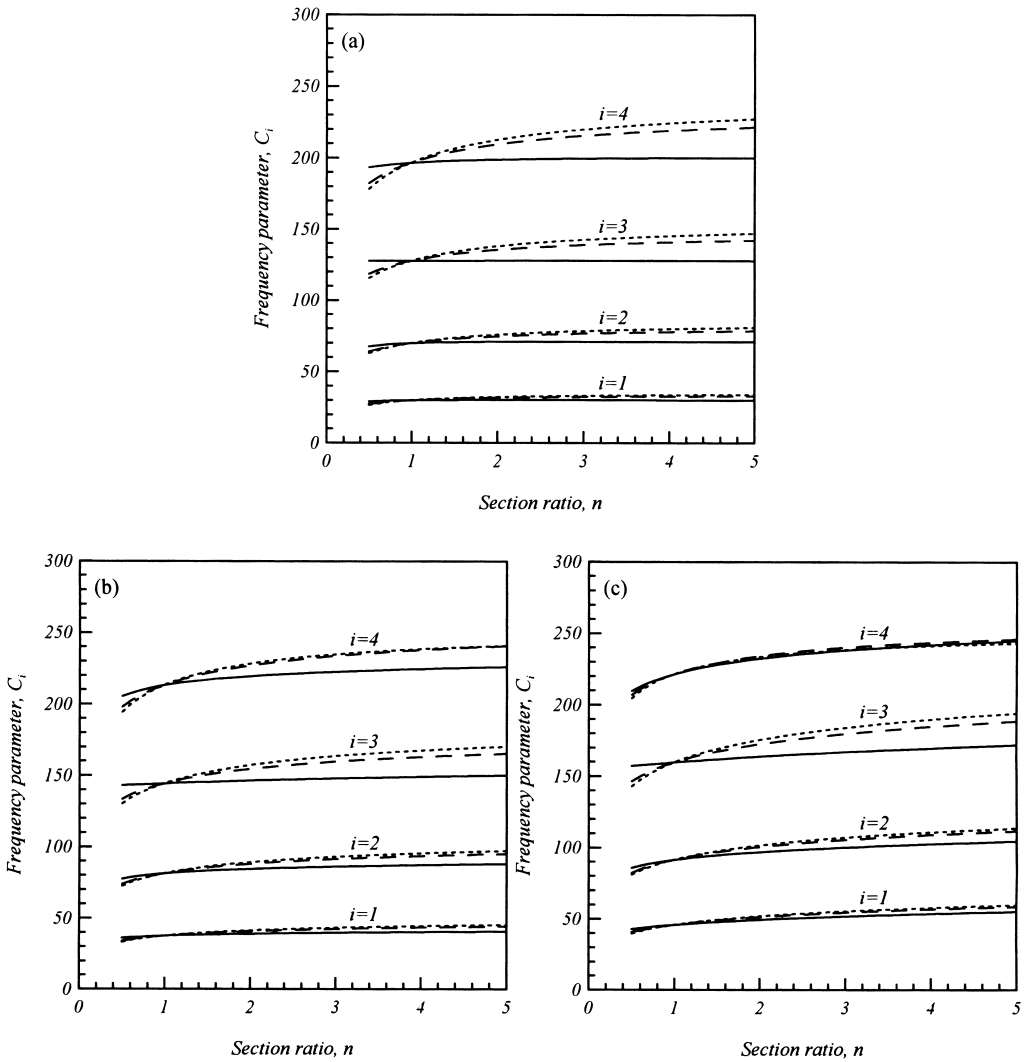

Fig. 8. Effect of n on frequency for parabolic arches: (a) hinged–hinged; (b) hinged–clamped; (c) clamped–clamped. Key as Fig. 6; $f = 0.2$; $s = 200$.

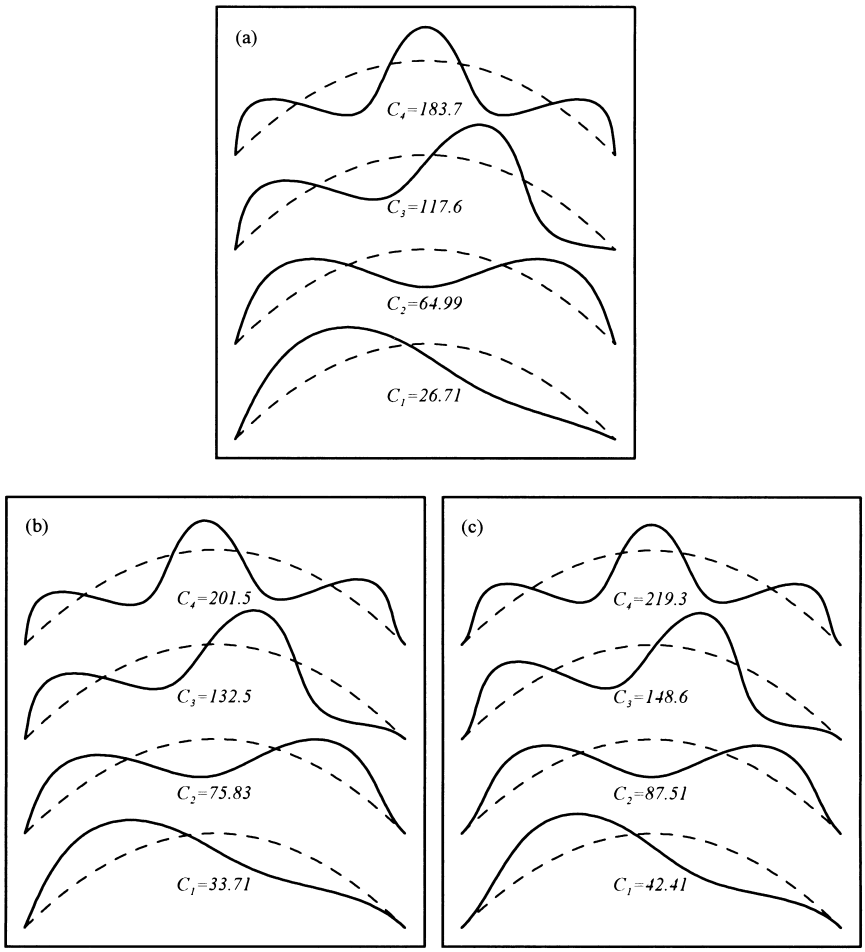

Fig. 9. Examples of mode shape for parabolic arches: (a) hinged–hinged; (b) hinged–clamped; (c) clamped–clamped. Breadth taper; $f = 0.25$; $s = 200$; $n = 1.5$.

along the top of each arch were used. To one of these reference points, on the underside of the arch was affixed a miniature accelerometer mounted so that it was sensitive only to radial arch acceleration. In a typical experiment, a hammer also fitted with a miniature accelerometer was struck at each of the reference points, in-plane and in the radial direction of the arch. All acceleration data were received by a Signal Analyzer (Model SD390, Scientific-Atlanta Corp.), and processed through a minicomputer using a fast Fourier transform (FFT) analyzer. For the details of data reduction, see Ewins (1985).

The data analysis lead to two important results: (1) the frequency dependent Frequency Response Function (FRF) defined as the ratio of the magnitude of the FFT for arch acceleration to the magnitude of the FFT for the hammer acceleration; and (2) the radial displacement mode shapes for the arch at the peaks of the FRF. The FRF for each of the three arches that we tested is shown in Fig. 10. The software gave a listing of the four lowest frequencies that corresponded to the first four peaks of each Frequency Response Function. These results, which we reproduced to within about 2% in repeated tests, are the measured frequencies listed in Table 3.

Considering all of these data, the measured frequencies averaged about 11% less than those predicted from theory. Especially, the measured frequencies for $i = 1$ averaged about 7% lower than the predicted values. The differences between theory and experiment are of the same order as obtained on uniform arches (Lee and Wilson, 1989) and may be accounted for, by several factors: the experimental difficulties of achieving "perfect" hammer strikes exactly on the arch centerline, where imperfect hammer strikes led to out-of-plane free vibrations; difficulties of achieving the ideal end constraint conditions (clamped or hinged); and the presence of natural structural damping in the experiments which was not included in the theoretical model.

From Table 3, it is found that the discrepancy between analytical and experimental values for C_3 of parabolic arch with hinged–hinged and hinged–clamped end constraints is relatively large. The main reason of the large discrepancy may be accounted for the looseness of the end hinges.

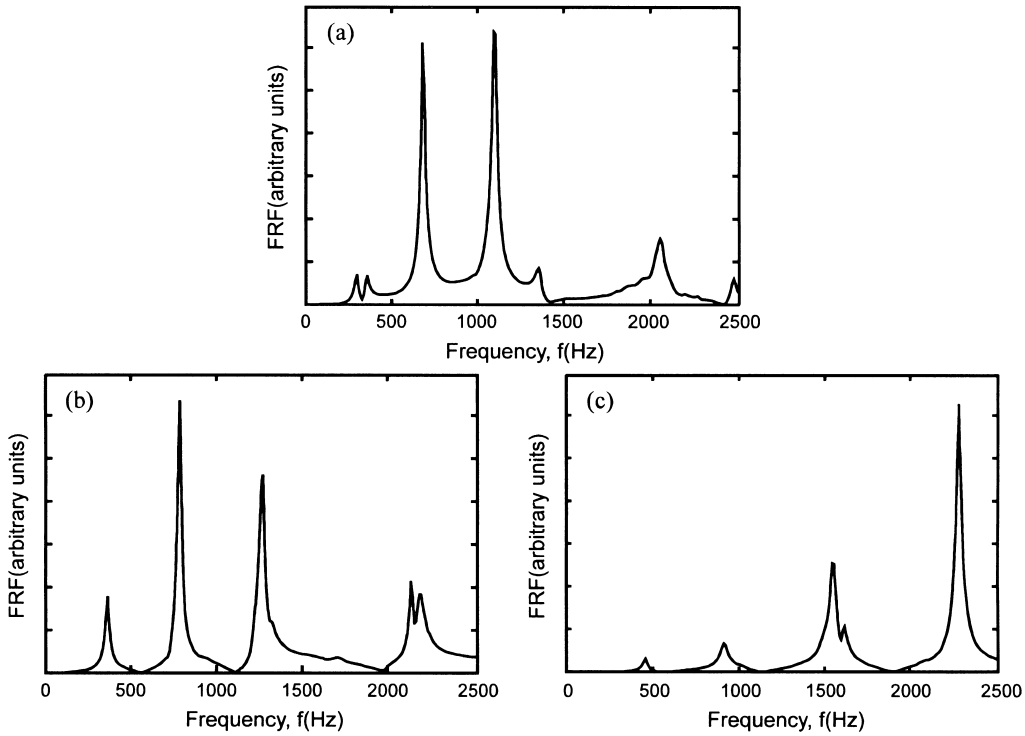

Fig. 10. Frequency Response Function of acceleration for experimental arches. (a) Hinged–hinged; (b) hinged–clamped; (c) clamped–clamped.

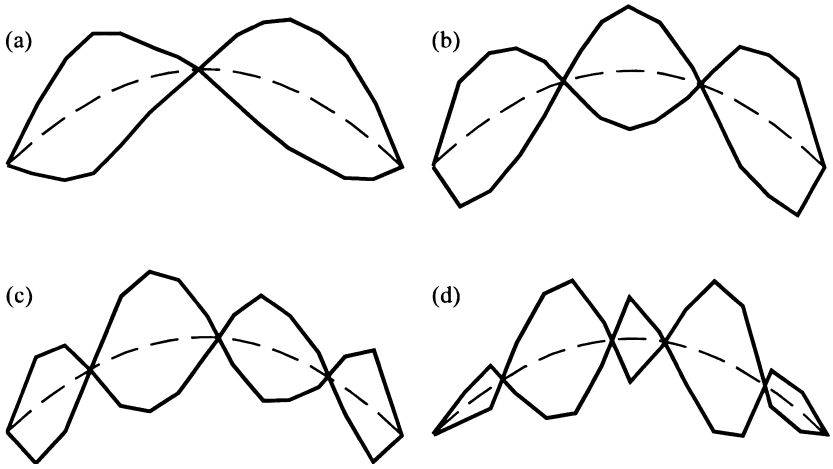

Fig. 11. Measured mode shapes of the hinged–hinged experimental arch. (a) Mode 1, 297 Hz; (b) mode 2, 684 Hz; (c) mode 3, 1100 Hz; (d) mode 4, 2049 Hz. – – – – – Undeformed arch.

The first four mode shapes as computed from the experimental data for the hinged–hinged arch are shown in Fig. 11. In reality, these measured shapes should be smooth; but the software that we used, simply connected data from the 15 reference points with straight lines. However, we observe that the general shapes agree with the computed results shown in Fig. 9(a). Not shown herein are the experimental mode shape data for the hinged–clamped and the clamped–clamped configurations. We observed that these measured results were in complete agreement with the corresponding computed results shown in Fig. 9(b) and (c).

7. Concluding remarks

The methods presented here for calculating frequencies and mode shapes for non-circular arches with non-uniform cross-section were found to be efficient and reliable over a wide range of system parameters. For three arch geometries (parabolic, catenary and elliptic), the effects of each of the three parameters f, s and n on C_i were investigated. For the parabolic arches, the effects of the type of taper on C_i were analyzed. Numerical results show that the arch geometry has little effect on the frequency parameters C_i, other parameters remaining the same. The frequency parameters C_i generally increase, as the type of taper changes from the breadth- to the square- to the depth-taper. Experiments in which four frequencies were measured on breadth-tapered quadratic arches with hinged–hinged, hinged–clamped and clamped–clamped ends, served to validate the results of the theoretical analysis.

Acknowledgements

The first author extends his thanks to the Korea Science and Engineering Foundation for financial support; and to Korea Advanced Institute of Science and Technology for providing the facilities and the appointment of Post-Doctoral Fellow to do this research in 1997.

References

Borg, S.F., Gennaro, J.J., 1959. Advanced Structural Analysis. Van Nostrand, Princeton, NJ.

Den Hartog, J.P., 1928. The lowest natural frequency of circular arcs. Philosophical Magazine 5, 400–408.

Ewins, D.J., 1985. Modal Testing: Theory and Practice. Wiley, New York.

Gupta, A.K., 1985. Vibration of tapered beams. Journal of Structural Engineering (ASCE) 111, 19–36.

Gupta, A.K., Howson, W.P., 1994. Exact natural frequencies of plane structures composed of slender elastic curved members. Journal of Sound and Vibration 175, 145–157.

Gutierrez, R.H., Laura, P.A.A., Rossi, R.E., Bertero, R., Villaggi, A., 1989. In-plane vibrations of non-circular arcs of non-uniform cross-section. Journal of Sound and Vibration 129, 181–200.

Henrych, J., 1981. The Dynamics of Arches and Frames. Elsevier, Amsterdam.

Irie, T., Yamada, G., Tanaka, K., 1983. Natural frequencies of in-plane vibration of arcs. Journal of Applied Mechanics (ASME) 50, 449–452.

Kang, K., Bert, C.W., Striz, A.G., 1995. Vibration analysis of shear deformable circular arches by the differential quadrature method. Journal of Sound and Vibration 181, 353–360.

Kawakami, M., Sakiyama, T., Matsuda, H., Morita, C., 1995. In-plane and out-of-plane free vibrations of curved beams with variable cross sections. Journal of Sound and Vibration 187, 381–401.

Laura, P.A.A., Verniere de Irassar, P.L., Carnicer, R., Bertero, R., 1988. A note on vibrations of a circumferential arch with thickness varying in a discontinuous fashion. Journal of Sound and Vibration 120, 95–105.

Lee, B.K., Wilson, J.F., 1989. Free vibrations of arches with variable curvature. Journal of Sound and Vibration 136, 75–89.

Leontovich, V., 1969. Frames and Arches. McGraw-Hill, New York.

Maurizi, M.J., Belles, P.M., Rossi, R.E., De Rosa, M.A., 1993. Free vibration of a three-centered arc clamped at the ends. Journal of Sound and Vibration 161, 187–189.

Romanelli, E., Laura, P.A.A., 1972. Fundamental frequencies of non-circular, elastic, hinged arcs. Journal of Sound and Vibration 24, 17–22.

Veletsos, A.S., Austin, W.J., Pereira, C.A.L., Wung, S.J., 1972. Free in-plane vibration of circular arches. Journal of the Engineering Mechanics Division (ASCE) 98, 311–329.

Volterra, E., Morell, J.D., 1960. A note on the lowest natural frequency of elastic arcs. Journal of Applied Mechanics (ASME) 27, 744–746.

Wang, T.M., 1972. Lowest natural frequency of clamped parabolic arc. Journal of the Structural Division (ASCE) 98, 407–411.

Wang, T.M., Moore, J.A., 1973. Lowest natural extensional frequency of clamped elliptic arcs. Journal of Sound and Vibration 30, 1–7.

Wang, T.M., 1975. Effect of variable curvature on fundamental frequency of clamped parabolic arcs. Journal of Sound and Vibration 41, 247–251.

Wilson, J.F., Lee, B.K., 1995. In-plane free vibrations of catenary arches with unsymmetric axes. Structural Engineering and Mechanics 3, 511–525.

Yildirim, V., 1997. A computer program for the free vibration analysis of elastic arcs. Computers and Structures 62, 475–485.